PAPER

Check for updates

Dry reforming of methane over single-atom Rh/Al₂O₃ catalysts prepared by exsolution†

Martijn J. Mekkering, [iD]ᵃ Jasper Biemolt, [iD]ᵃ Jeen de Graaf,ᵃ Yi-An Lin,ᵃ
Nicolaas P. van Leest,ᵃ Alessandro Troglia, [iD]ᵇ Roland Bliem, [iD]ᵇᶜ Bas de Bruin, [iD]ᵃ
Gadi Rothenberg [iD]*ᵃ and Ning Yan [iD]*ᵃ

Single-atom catalysts often show exceptionally high performance per metal loading. However, the isolated atom sites tend to agglomerate during preparation and/or high-temperature reaction. Here we show that in the case of Rh/Al₂O₃ this deactivation can be prevented by dissolution/exsolution of metal atoms into/from the support. We design and synthesise a series of single-atom catalysts, characterise them and study the impact of exsolution in the dry reforming of methane at 700–900 °C. The catalysts' performance increases with increasing reaction time, as the rhodium atoms migrate from the subsurface to the surface. Although the oxidation state of rhodium changes from Rh(III) to Rh(II) or Rh(0) during catalysis, atom migration is the main factor affecting catalyst performance. The implications of these results for preparing real-life catalysts are discussed.

Introduction

The worldwide scarcity of noble metals and the need for highly selective catalytic processes are driving increased interest in single-atom catalysts (SACs).[1–4] These catalysts have the highest surface-to-volume ratio, and often show different chemoselectivity compared to traditional supported nanoparticles.[5–8] In fact, they form a bridge between homogeneous and heterogeneous catalysis, with the potential benefits of both disciplines.

SACs are usually prepared by impregnating inorganic metal complexes on porous supports followed by thermal decomposition.[9–11] They can also be prepared by more sophisticated methods, namely chemical vapor deposition, atomic layer deposition and plasma treatment, though scaling up these methods is problematic. Like conventional supported nanoparticle catalysts, SACs suffer from sintering, which negates their activity and selectivity advantages.[12–14] Yet while conventional catalysts typically show nanoparticle migration on the surface, SACs show more often solid solvation and exsolution of active site atoms to/from the bulk.[12]

Things get more complicated when we consider the catalytic reactions themselves. Reactions such as dry reforming, steam reforming, and dehydrogenation[13] typically require high temperatures, which cause exsolution and re-distribution of the active sites. Yet when you characterize such catalysts, typically after cooling them down and preparing samples, the active atoms may diffuse back into the bulk.

In this paper, we study the factors that govern the dynamics of atom migration on the surface and subsurface of supported SACs. Our benchmark reaction is the dry reforming of methane, running at 700–900 °C. We use metal exsolution to improve the catalyst efficiency.[14,15] Importantly, this approach also works for non-reducible metal oxide supports.[16] To the best of our knowledge, this is the first report that studies the effects of SAC exsolution and migration on catalyst performance on Rh/Al₂O₃ complexes.

Experimental

Materials and instrumentation

All chemicals were purchased from commercial sources and used as received. Online gas chromatography was measured on a Global Analyser Solutions Compact GC4.0 instrument equipped with two columns (Molsieve 0.32 mm and RT-Q-BOND fused silica, 0.32 mm) and a thermal conductivity detector. X-ray diffraction (XRD) patterns were obtained with a MiniFlex II diffractometer using Ni-filtered CuKα radiation, ranging from 10° to 70°. The X-ray tube was operated at 30 kV and 15 mA, with a 2.5° step and 1 s dwell time. Electron paramagnetic resonance (EPR) measurements were performed on a Bruker EMX-Plus CW X-band EPR spectrometer which was equipped with an ER 4112 HV-CF100

ᵃ *Van't Hoff Institute for Molecular Sciences, University of Amsterdam, Science Park 904, 1090 GD Amsterdam, The Netherlands. E-mail: g.rothenberg@uva.nl, n.yan@uva.nl; Web:* **www.hims.uva.nl/hcsc**
ᵇ *Advanced Research Center for Nanolithography, Science Park 106, 1098 XG Amsterdam, The Netherlands*
ᶜ *Van der Waals–Zeeman Institute, University of Amsterdam, Science Park 904, 1098 XH Amsterdam, The Netherlands*
† Electronic supplementary information (ESI) available. See DOI: https://doi.org/10.1039/d2cy02126a

This journal is © The Royal Society of Chemistry 2023

Catal. Sci. Technol., 2023, **13**, 2255–2260 | **2255**

He cryostat (10 K). CO-DRIFTS measurements were performed on a Nicolet iS-50 Fourier Transform infrared spectrometer, equipped with a mercury–cadmium–telluride (MCT) detector. A 4 cm^{-1} resolution was used, and the sample cup was loaded with the catalyst in a Harrick praying mantis. Samples were pretreated with a high temperature vacuum ($T = 300$ °C, $p = 10^{-9}$ bar) to ensure desorption of O_2 and H_2O, cooled down to room temperature and subsequently treated with CO until the chamber was saturated. The chamber was then depressurized to 10^{-9} bar, ensuring no residual CO, and then adsorption spectra were collected. Scanning electron microscopy (SEM) images were obtained on a JEOL JSM-6010LA microscope with an accelerating voltage of 10 kV. Transmission electron microscopy (TEM) images were obtained on a JEOL JEM-2011 microscope operating at an accelerating voltage of 200 kV, recorded using a Gatan 794 CCD camera. X-ray photoelectron spectroscopy (XPS) was performed using a Scienta Omicron R4000 HiPP-3 analyzer (swift acceleration mode, 1 mm slit entrance) and a monochromatic Al-Kα source (1486.6 eV, base pressure lower than 1.0×10^{-9} mbar). Adventitious carbon was used as reference peak. ICP analysis was performed by Kolbe Labs GmbH.

Procedure for catalyst preparation

Example: 0.5 wt% Rh/alumina: a stock solution of Rh precursor was prepared by dissolving 12.5 mg $RhCl_3\cdot 3H_2O$ (Strem Chemical Inc., 40% Rh) in 20 mL deionized water at room temperature. Then, 1 g of γ-alumina was added, which was pre-ground and dried. The suspension was dried in a rotary evaporator at 45 °C, 40 mbar, 150 rpm for 1–2 h (slow drying is needed to prevent nanoparticle formation during solvent evaporation). The resulting powder was then further dried and subsequently calcined in static air at 800 °C for 4 h with a ramp rate of 5 °C min^{-1}, followed by reduction *in situ* in a 95 : 5 $N_2 : H_2$ mixture at 600 °C for 1 h, see left photo in Fig. 1 (the right photo shows the same catalyst after coking has occurred in the reactor in the presence of methane).

The Pt/Al_2O_3 Ru/Al_2O_3 and Pd/Al_2O_3 catalysts were similarly prepared, starting from $Pt(NH_3)_4(NO_3)_2$ (Sigma-Aldrich), $RuCl_3\cdot H_2O$ (VWR, 40–43%), and K_2PdCl_4 (Sigma-Aldrich), respectively.
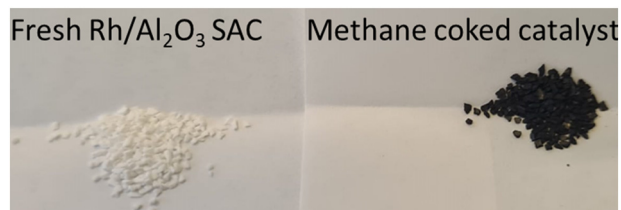
Fig. 1 Images of the fresh SAC and the coked catalyst after methane treatment at 900 °C. The differences due to coking (blackening) are significant.

Hot-quenching was performed by calcining the catalysts at 900 °C in air, 20 °C min^{-1} for 1 h and removing them to cool down to room temperature within a minute.

Acid wash experiments were carried out on a funnel equipped with a filter, using 120 mL 1 M HCl by gravity filtration. Samples were then washed with water until reaching pH = 7, and dried at 120 °C for 1 h.

Procedure for catalyst testing

All dry reforming reactions were performed in a plug-flow reactor. In a typical experiment, 70 mg crushed and sieved (435–530 μm) catalyst was weighed and put in a quartz tube fitted with a glass frit ($\frac{1}{4}$ inch diameter, 450 mm length, *ca.* 1 cm catalyst bed length). After *in situ* reduction at 600 °C, the catalyst was heated to the desired temperature (typically 700 °C) under a nitrogen atmosphere. The reactant gas composition, $CH_4 : CO_2 : N_2 = 1 : 1 : 8$, was selected at $T = 700$ °C in a total flow rate of 100 mL min^{-1}, corresponding to a gas-hourly space velocity of 8.57×10^4 mLh^{-1} gcat^{-1}. Each catalyst was tested at different temperatures, from 700 to 900 °C and back to 700 °C in steps of 50 °C, with a ramp rate of 5 °C min^{-1} when heating and −5 °C min^{-1} when cooling. At each temperature, the conversion and yield were measured for 30 min using gas chromatography. At the end of the sequence, the catalyst was cooled down gradually to room temperature under nitrogen atmosphere.

Results and discussion

First, we examined the dissolution properties of different noble metal SACs on alumina by preparing a set of M/Al_2O_3 catalysts (where M = Pt, Rh, Ru, Pd). Each synthesis followed the four steps of impregnation, drying, calcination and activation (see experimental section for details). Reaching the high dispersion of single-atom sites is not guaranteed, as it requires a good dissolution of the metal ions into the matrix during the calcination step. Then, during the activation step, the metal atoms can exsolve to the surface as single sites. Poor dissolution will cause more nanoparticle formation on the support surface, rather than forming a SAC. Rhodium showed excellent dissolution, with no nanoparticles observed on the surface. Conversely, the X-ray diffraction (XRD) patterns for the Pt, Pd and Ru/Al_2O_3 catalysts did show metal nanoparticles, indicating poor dissolution (Fig. 2a). We therefore focused on the Rh/Al_2O_3 catalyst (throughout this work we observed only the γ-alumina phase[17]).

Choosing the catalyst loading is tricky. Too low a loading will not show anything, while high loadings will mask any dissolution effect. Assuming that the atoms should be at least 2–3 atomic distances apart, we arrived at a theoretical density of *ca.* one atom per 4 nm². Then, using trial and error experiments, we found that a loading of 0.5 wt%, or one Rh atom per 3 nm² of alumina surface, was suitable.[18] Samples with this loading did not show Rh nanoparticles in XRD (Fig. 2a).
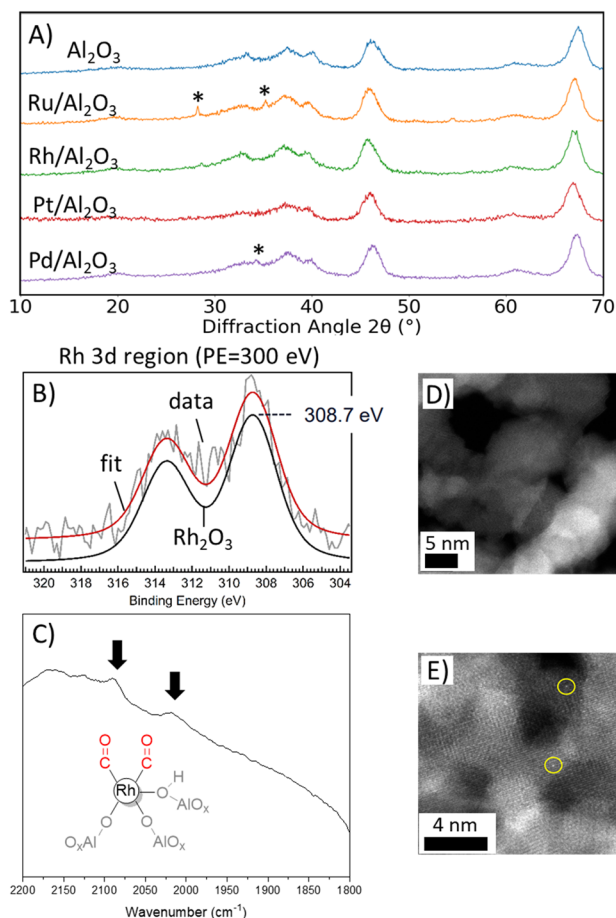
Fig. 2 (A) X-ray diffractograms of the 0.5 wt% noble metal on γ-Al$_2$O$_3$. Note the absence of Rh peaks, indicating Rh dissolution. (B) Rh 3d XP spectrum of the 0.5 wt% Rh/Al$_2$O$_3$ species which matches the electron binding energy of Rh$_2$O$_3$ (C). CO-DRIFTS on the Rh/Al$_2$O$_3$ species showing minimal Rh presence at the surface. (D) TEM image of 0.005 wt% Rh/Al$_2$O$_3$ without hot-quenching showing no Rh species. (E) TEM image of 0.005 wt% Rh/Al$_2$O$_3$ with hot-quenching showing Rh species at the surface.

Using the 0.5 wt% loading as our upper threshold, we focused on preparing Rh/Al$_2$O$_3$ single-atom catalysts with lower loadings, all the way down to 0.001 wt% (equivalent to one Rh atom per 1500 nm^2 of alumina surface). All catalysts were dried overnight to prevent agglomeration, and characterized using XRD, CO diffuse reflectance infrared Fourier-transform spectroscopy (CO-DRIFTS), high-resolution transmission electron microscopy (HRTEM) and X-ray photoelectron spectroscopy (XPS).

The CO-DRIFTS experiments confirmed the dissolution of the Rh atoms into the alumina framework (Fig. 2c; the peaks are in agreement with those reported by Christopher and co-workers[19]). Noble metal catalysts often suffer from CO poisoning,[20–22] and one would expect to see in the DRIFTS the linear Rh–CO bond vibration. We did not see this. Nor were any Rh species observed with HRTEM (see Fig. 2d), further confirming the dissolution of Rh atoms into the alumina bulk.

Importantly, the dynamics of atom migration are governed by the sample cooling rate. Fast cooling, or quenching, is known to induce material deformities.[23–25] Yet we show here that it also prevents the dissolution of single atoms back into the bulk. Whereas slow cooling allowed the Rh atoms to dissolve back into the alumina (see above and Fig. 2d), quenching left them on the surface (see AC-HRTEM image in Fig. 2e).

To see whether this dissolution of Rh atoms applies to other oxide supports, we ran a control experiment of CO-DRIFTS on Rh/CeO$_2$ samples. Here, we saw the linearly bonded CO–Rh/CeO$_2$ peaks[26] without quenching the sample (see Fig. S4A,† this also fits with the fact that ceria is denser (7.13 g cm^{-3}) and less permeable than alumina (3.97 g cm^{-3}) at these temperatures[27]). Combined with the fact that Pt, Pd and Ru/Al$_2$O$_3$ did not show dissolution, we conclude that the metal atom dissolution into the support requires specific combinations.[28]

We then studied the effect of exsolution and dissolution of rhodium atoms on the catalytic activity. This was done by running sequential dry reforming experiments at T = 700–900 °C (DRM, eqn (1)). In this reaction, methane and CO$_2$ are thermocatalytically converted into syngas.[29] The catalysts often deactivate through coking, and an important advantage of using SACs is that they suppress coke formation.[30–34]

$$CH_4 + CO_2 \rightarrow 2CO + 2H_2 \quad \Delta H^0_{298K} = +247 \text{ kJ mol}^{-1} \quad (1)$$

Exsolution is best observed at the catalyst operating limit, where the effect of the additional exsolved atoms is more visible (if there are already many active sites on the surface, e.g. at high loadings, the additional exsolved atoms won't make such a difference).[35] Therefore, we measured the turnover frequencies (mol CO produced per mol Rh per second) for different Rh loadings (Fig. 3a). We saw that 0.005 wt% was the optimal loading at 850 °C. The Rh loading was confirmed by ICP analysis (found 0.0041 wt%, calcd 0.005 wt%). This loading, which was used henceforth throughout this work, is low enough to compete on cost with a commercial 10 wt% Ni/Al$_2$O$_3$ catalyst (cf. cost analysis in Fig. S2b†).

We then studied the catalytic performance by monitoring the CO yield at varying temperatures (Fig. 3b, the CO yield was calculated according to eqn S1 in the ESI†). The increased yield at higher temperatures confirmed the endothermicity of the reaction. It also matched the theoretical thermodynamic yields calculated for the surface-saturated 0.5 wt% M/Al$_2$O$_3$ combinations (Fig. S2a†). The ramping from 700 °C to 900 °C and back was done to verify that changing the temperature influences the exsolution. Re-running the experiment improved the catalytic activity, as the repeated heating of the catalyst to 900 °C increased its performance (cf. 2nd and 3rd runs in Fig. 3b). These results support our Rh exsolution hypothesis, with maximal exsolution occurring at 900 °C. This was further supported by additional runs (Fig. S3a†)
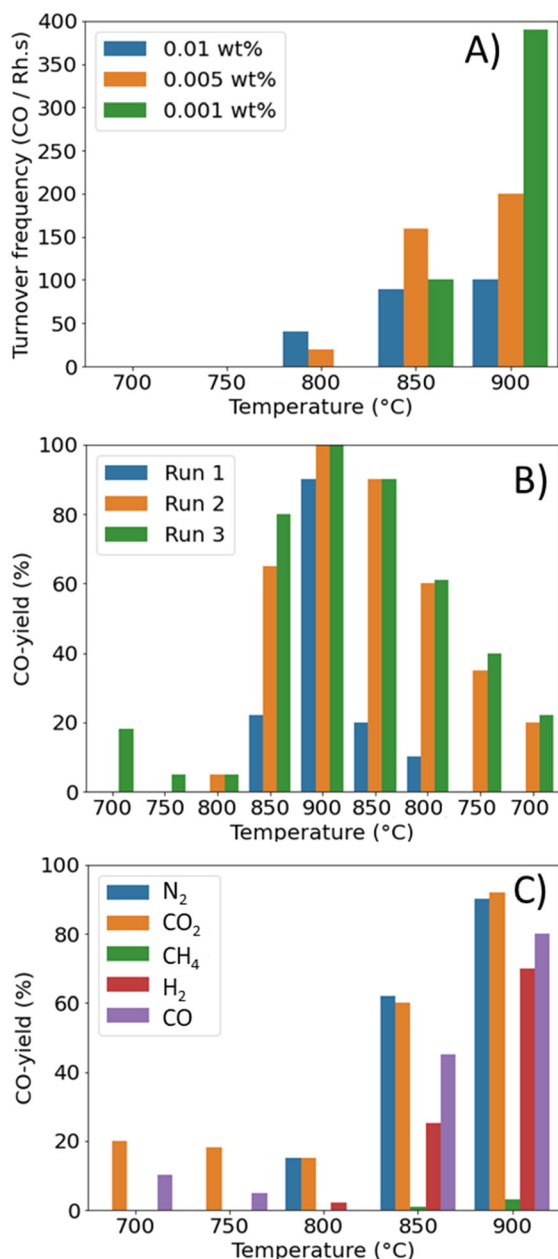
Fig. 3 (A) Turnover frequencies for different Rh/Al_2O_3 catalyst loadings in DRM. (B) Three consecutive DRM runs in the presence of a 0.005 wt% Rh/Al_2O_3 catalyst sample, showing the increased yield and stability at 850 °C after the first run. (C) Temperature-dependent yields after treating samples of 0.005 wt% Rh/Al_2O_3 catalysts with different gasses as indicated. Pretreatment with CH_4 led to coking, blocking the active sites and giving <3% yield. Note the decreased performance of hydrogen-treated catalysts compared to the nitrogen-treated ones.

albeit that the stability of the SACs at 900 °C was lower (Fig. S3b†).

Elsewhere, Tomida and Haneda showed that rhodium aluminate ($RhAlO_x$) species may form on the surface at these high temperatures.[36] Yet they also observed that such species reduce the catalytic activity, which we do not see here. We therefore suggest that part of the activity increase may be due to the removal of $RhAlO_x$ species on the surface, leaving

highly efficient SACs, in agreement with the results of Li and co-workers.[37]

Nanocluster formation at such temperatures is very common, and could explain the change in performance after treatment at 900 °C. To test this hypothesis, we ran a high temperature pre-treatment of the catalyst samples under different gasses, before testing these in DRM. The overall performance varied depending on the gas (Fig. 3c). Nanoclusters are more likely to form in reducing atmospheres than in neutral or oxidizing ones.[14,15] We therefore compared the performance of catalysts treated in N_2 and H_2 to identify whether the active components were SACs or nanoclusters (all other conditions were identical). Indeed, we found that hydrogen pre-treatment lowered the CO yield by 20%. Interestingly, pre-treatment with methane lowered the catalyst performance to that of the plain alumina background reaction, indicating a complete blocking of the rhodium sites by coking (visible to the naked eye in this case, see photos in Fig. 1). We attribute this to the decomposition of methane, acting as a reducing agent as well as a source of coke carbon at these high temperatures.

The higher catalytic activity after the first run could reflect the presence of more single-atom sites on the surface *via* exsolution. Alternatively, it may be due to changes in the metal oxidation states. To measure the latter, we used electron paramagnetic resonance (EPR) spectroscopy. Comparing the EPR spectra of pristine catalyst samples with those of spent ones (after the first reaction cycle), shows a transition from a single peak (triplet at $g \approx 4.3$) in the pristine state to multiple peaks (doublet at $g \approx 2$) in the activated catalyst (Fig. 4a). Simulation afforded $g_{11} = 2.016$, $g_{22} = 2.001$ and $g_{33} = 1.901$, showing a hyperfine coupling interaction with ^{103}Rh ($I = \frac{1}{2}$ nucleus; $A^{Rh}_{11} = 68$ MHz). The simulation of hyperfine coupling with the nucleus ^{103}Rh matched the experimental spectra. The hyperfine coupling and the formation of a doublet spin state both support the reduction of Rh_2O_3 to lower-valent rhodium (RhO or isolated Rh(0) atoms).

Control experiments using a 1 M HCl acid wash confirmed the removal of surface-bonded Rh under acid wash (*cf.* EPR spectra in Fig. 4a). Testing these catalysts in dry reforming indeed showed a reduced performance, with an increased activity for activated samples (Fig. 4b).

The extent of Rh atom migration and its impact on the DRM activity was estimated by preparing $Rh/Al_2O_3@Al_2O_3$ core–shell microstructures on co-precipitated Rh/Al_2O_3 catalysts. This gave structures comprising 25 wt% Rh/Al_2O_3 and 75 wt% Al_2O_3 (6 nm thick shell[38]) with minimal catalytic activity (Fig. 3c). Despite its higher nominal loading, this catalyst performed worse than the 0.001 wt% Rh/Al_2O_3 catalyst (*cf.* with Fig. 2a, green bar). Activating the sample at 900 °C for 12 h under CO_2 atmosphere (which increased the performance as shown in Fig. 3c), yielded only a minimal increase in activity (Fig. 4c). This confirms that atom migrations are more important than oxidation state changes. These migrations are typically to/from the immediate
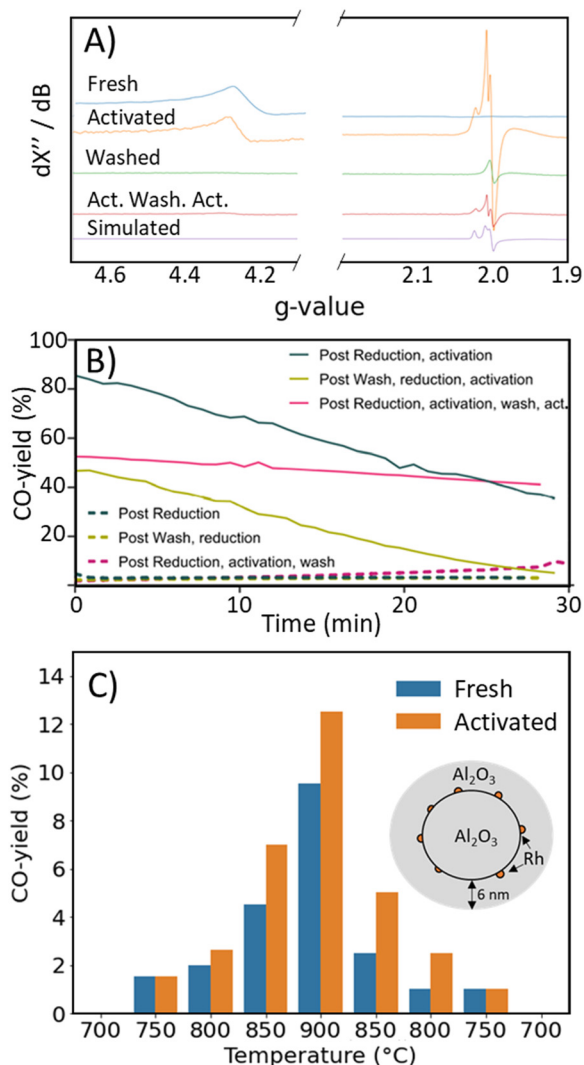
Fig. 4 (A) EPR measurements on the 0.005 wt% Rh/Al_2O_3 catalysts. Note the difference in peaks for the fresh catalyst, compared to the activated catalyst. The peak intensity at $g = 2.01$ and $g = 2.024$ decreased after acid washing and disappeared. After activation of the washed catalyst, the peaks match the originally activated catalyst whereas only a decreased intensity was observed. (B) The effects of the different treatments on the performance in DRM. (C) The performance of alumina-overcoated Rh/Al_2O_3 catalysts, showing only minimal improvement in activity after activation.

subsurface layer (~1 nm), in agreement with theoretical studies. In principle, the CO yield can be improved by reducing the shell thickness or by increasing the activation treatment period.[39]

Conclusions

Formation of SACs by dissolution/exsolution of metal atoms is metal- and lattice-specific. It occurs readily in the case of Rh/Al_2O_3 at 700–900 °C, but not for other platinum group metal-support combinations. Two processes are at play here: one is the classical lateral migration of metal atoms and clusters across the surface, which decreases the catalytic

performance due to agglomeration. The other is the dissolution/exsolution of single atoms to/from the immediate subsurface, which yields in active SACs. Under the reducing conditions of DRM, Rh(III) ions are reduced to Rh(II) or Rh(0), but these oxidation state changes are less important compared to the atom migration processes. Overall, these findings have important implications for SAC synthesis protocols: starting from lower-loading formulations, the surface coverage of which can be calculated *a priori*, can favor the dissolution/exsolution route over the lateral migration, thus increasing catalyst stability.

Author contributions

Conflicts of interest

Acknowledgements

Notes and references

1 Y. Shang, X. Duan, S. Wang, Q. Yue, B. Gao and X. Xu, *Chin. Chem. Lett.*, 2021, **33**, 663–673.

2 S. Yang, J. Kim, Y. J. Tak, A. Soon and H. Lee, *Angew. Chem., Int. Ed.*, 2016, **55**, 2058–2062.

3 X. Hai, S. Xi, S. Mitchell, K. Harrath, H. Xu, D. F. Akl, D. Kong, J. Li, Z. Li, T. Sun, H. Yang, Y. Cui, C. Su, X. Zhao, J. Li, J. Pérez-Ramírez and J. Lu, *Nat. Nanotechnol.*, 2022, **17**, 174–181.

4 J. L. J. Lin, A. Wang, B. Qiao, X. Liu, X. Yang, X. Wang, T. Z. J. Li and J. Liu, *J. Am. Chem. Soc.*, 2013, **135**, 15314–15317.

5 Z. Li, X. Dong, M. Zhang, L. Leng, W. Chen, J. H. Horton, J. Wang, Z. Li and W. Wu, *ACS Appl. Mater. Interfaces*, 2020, **12**, 57569–57577.

6 B. Qiao, J. X. Liang, A. Wang, C. Q. Xu, J. Li, T. Zhang and J. J. Liu, *Nano Res.*, 2015, **8**, 2913–2924.

7 B. Q. F. Chen, X. Jiang, L. Zhang and R. Lang, *Chin. J. Catal.*, 2018, **39**, 893–898.

8 G. Spezzati, A. D. Benavidez, A. T. DeLaRiva, Y. Su, J. P. Hofmann, S. Asahina, E. J. Olivier, J. H. Neethling, J. T. Miller, A. K. Datye and E. J. M. Hensen, *Appl. Catal., B*, 2019, **243**, 36–46.

This journal is © The Royal Society of Chemistry 2023

Catal. Sci. Technol., 2023, **13**, 2255–2260 | **2259**

9 B. Qiao, J. Liu, Y. G. Wang, Q. Lin, X. Liu, A. Wang, J. Li, T. Zhang and J. Liu, *ACS Catal.*, 2015, **5**, 6249–6254.

10 P. Xie, T. Pu, A. Nie, S. Hwang, S. C. Purdy, W. Yu, D. Su, J. T. Miller and C. Wang, *ACS Catal.*, 2018, **8**, 4044–4048.

11 K. Yuan, Y. Guo, L. Huang, L. Zhou, H. J. Yin, H. Liu, C. H. Yan and Y. W. Zhang, *Inorg. Chem.*, 2021, **60**, 4207–4217.

12 L. Lin, Z. Chen and W. Chen, *Nano Res.*, 2021, **14**, 4398–4416.

13 S. Gómez-Quero, T. Tsoufis, P. Rudolf, M. Makkee, F. Kapteijn and G. Rothenberg, *Catal. Sci. Technol.*, 2013, **3**, 962–971.

14 C. Tang, K. Kousi, D. Neagu, J. Portolés, E. I. Papaioannou and I. S. Metcalfe, *Nanoscale*, 2019, **11**, 16935–16944.

15 T. Cao, O. Kwon, R. J. Gorte and J. M. Vohs, *Nanomaterials*, 2020, **10**, 1–23.

16 K. A. Ledwa, L. Kępiński and M. Pawlyta, *ChemNanoMat*, 2020, **6**, 1260–1269.

17 Q. Yuan, Z. Zhou, J. Zhuang and X. Wang, *Inorg. Chem.*, 2010, **49**, 5515–5521.

18 T. K. Slot, N. Riley, N. R. Shiju, J. W. Medlin and G. Rothenberg, *Chem. Sci.*, 2020, **11**, 11024–11029.

19 E. K. Schroeder, J. Finzel and P. Christopher, *J. Phys. Chem. C*, 2022, **126**, 18292–18305.

20 F. Lyu, M. Cao, A. Mahsud and Q. Zhang, *J. Mater. Chem. A*, 2020, **8**, 15445–15457.

21 C. Lamy, *Electrochim. Acta*, 1984, **29**, 1581–1588.

22 N. J. B. Q. Li, R. He, J.-A. Gado and J. O. Jensen, *J. Electrochem. Soc.*, 2003, **150**, A1599–A1605.

23 P. De Hey, J. Sietsma and A. Van Den Beukel, *Acta Mater.*, 1998, **46**, 5873–5882.

24 D. K. J. Wang, *J. Compos. Mater.*, 2000, **34**, 1456–1471.

25 L. P. F. Auricchio, *Int. J. Numer. Methods Eng.*, 2004, **61**, 807–836.

26 H. Zhu, Y. Li and X. Zheng, *Appl. Catal., A*, 2019, **571**, 89–95.

27 A. Martínez-Arias, M. Fernández-García, L. N. Salamanca, R. X. Valenzuela, J. C. Conesa and J. Soria, *J. Phys. Chem. B*, 2000, **104**, 4038–4046.

28 C. Hernandez-Mejia, E. S. Gnanakumar, A. Olivos-Suarez, J. Gascon, H. F. Greer, W. Zhou, G. Rothenberg and N. R. Shiju, *Catal. Sci. Technol.*, 2016, **6**, 577–582.

29 E. Devid, D. Zhang, D. Wang, M. Ronda-Lloret, Q. Huang, G. Rothenberg, N. R. Shiju and A. W. Kleyn, *Energy Technol.*, 2020, **8**, 1900886.

30 M. J. Hülsey, B. Zhang, Z. Ma, H. Asakura, D. A. Do, W. Chen, T. Tanaka, P. Zhang, Z. Wu and N. Yan, *Nat. Commun.*, 2019, **10**, 1–10.

31 R. Franz, T. Kühlewind, G. Shterk, E. Abou-Hamad, A. Parastaev, E. Uslamin, E. J. M. Hensen, F. Kapteijn, J. Gascon and E. A. Pidko, *Catal. Sci. Technol.*, 2020, **10**, 3965–3974.

32 R. L. B. A. Medeiros, G. P. Figueredo, H. P. Macedo, Â. A. S. Oliveira, R. C. Rabelo-Neto, D. M. A. Melo, R. M. Braga and M. A. F. Melo, *Fuel*, 2020, **287**, 1–11.

33 A. A. Ibrahim, A. S. Al-Fatesh, W. U. Khan, S. O. Kasim, A. E. Abasaeed, A. H. Fakeeha, G. Bonura and F. Frusteri, *Int. J. Hydrogen Energy*, 2019, **44**, 27784–27794.

34 S. Das, M. Sengupta, A. Bag, A. Saini, M. Muhler and A. Bordoloi, *ACS Appl. Nano Mater.*, 2021, **4**, 2547–2557.

35 D. Pawanpreet Kour, I. Ahmed, S. Sharma, S. K. Sharma, K. Yadav and Y. K. Mishra, *ChemCatChem*, 2022, 1–64.

36 Y. Tomida and M. Haneda, *Catal. Today*, 2021, **376**, 81–86.

37 C. H. Li, J. Wu, A. B. Getsoian, G. Cavataio and J. R. Jinschek, *Chem. Mater.*, 2022, **34**, 2123–2132.

38 A. Eftekhari, B. Modahedi, G. Dini and M. Milani, *J. Eur. Ceram. Soc.*, 2018, **38**, 3297–3304.

39 M. J. Louwerse and G. Rothenberg, *ACS Catal.*, 2013, **3**, 1545–1554.

This journal is © The Royal Society of Chemistry 2023